# Adjoint-based sensitivity analysis for a numerical storm surge model

Simon C. Warder[a,*], Kevin J. Horsburgh[b], Matthew D. Piggott[a]

[a] *Department of Earth Science and Engineering, Imperial College London, London, SW7 2AZ, UK*
[b] *National Oceanography Centre, Liverpool, L3 5DA, UK*

**Abstract**

Numerical storm surge models are essential to forecasting coastal flood hazard and informing the design of coastal defences. However, such models rely on a variety of inputs, many of which carry uncertainty, and an awareness and understanding of the sensitivity of the model outputs with respect to those uncertain inputs is necessary when interpreting model results. Here, we use an unstructured-mesh numerical coastal ocean model, *Thetis*, and its adjoint, to perform a sensitivity analysis for a hindcast of the $5^{\text{th}}/6^{\text{th}}$ December 2013 North Sea surge event, with respect to the bottom friction coefficient, bathymetry and wind stress forcing. The results reveal spatial and temporal patterns of sensitivity, providing physical insight into the mechanisms of surge generation and propagation. For example, the sensitivity of the skew surge to the bathymetry reveals the protective effect of a sand bank off the UK east coast. The results can also be used to propagate uncertainties through the numerical model; based on estimates of model input uncertainties, we estimate that modelled skew surges carry uncertainties of around 5 cm and 15 cm due to bathymetry and bottom friction, respectively. While these uncertainties are small compared with the typical spread in an ensemble storm surge forecast due to uncertain meteorological inputs, the adjoint-derived model sensitivities can nevertheless be used to inform future model calibration and data acquisition efforts in order to reduce uncertainty. Our results demonstrate the power of adjoint methods to gain relevant insight into a storm surge model, providing information complementary to traditional ensemble uncertainty quantification methods.

*Keywords:* Storm surge, Adjoint, Sensitivity analysis, Uncertainty quantification, Unstructured mesh, Finite element method

*Corresponding author
*Email addresses:* s.warder15@imperial.ac.uk (Simon C. Warder), kevinh@noc.ac.uk (Kevin J. Horsburgh), m.d.piggott@imperial.ac.uk (Matthew D. Piggott)

## 1. Introduction

Storm surge poses a significant hazard for coastal communities worldwide. Allowing for investment in adaptation measures (e.g. rising flood defences), global flood losses in 136 of the world's largest coastal cities have recently been estimated to rise from US$6 bn per year in 2005 to US$60-63 bn per year in 2050 (Hallegatte et al., 2013). Globally, the increase in extreme sea levels (Stocker et al., 2013) will result in critical flood defence thresholds being reached more frequently and therefore the risk of flooding will increase. The UK is vulnerable to storm surges, particularly along its North Sea coast; a large number of severe storms have impacted the UK in the last century (Haigh et al., 2016), with the two most severe of those events occurring in the North Sea in 1953 and 2013. The approximate economic impacts of the coastal flooding resulting from these events (for year 2014) were £1.2 bn and £0.25 bn respectively; the impact of the latter event was reduced through mitigation action taken after the 1953 event (Wadey et al., 2015). With continued development of the coastal zone in flood risk areas (ASC, 2014), the role of storm surge modelling remains vital.

Essential to the intelligent application of any storm surge model is an understanding of the model's sensitivity to its uncertain inputs. In a forecast scenario, the greatest model uncertainty arises from the meteorological forcing, namely the surface stress due to wind, and the atmospheric pressure gradient. For this reason, it is common to employ ensemble methods for uncertainty quantification, whereby the surge model is run multiple times, with each run using a different sample from the uncertain distribution of meteorological inputs (Flowerdew et al., 2010). While such ensemble methods provide a practical approach to uncertainty quantification within an operational forecast framework, they provide little insight into the patterns (in space and/or time) of the underlying model sensitivity, and they depend on the choice of meteorological ensemble.

An alternative approach to sensitivity analysis is provided by adjoint methods. In the context of numerical modelling, adjoint methods are used to efficiently compute gradients of model outputs with respect to model inputs, which can in principle vary in both space and time. Such methods have been used within a meteorological context since the 1980s (e.g. Hall et al. (1982)), and have a variety of applications within the field of coastal ocean modelling. Adjoint-derived sensitivities to model inputs can be used for gaining physical insight into a modelled system (e.g. Losch and Heimbach (2007), Massmann (2010), Verdy et al. (2014), Nowak (2015), Villaret et al. (2016)), or can be used within frameworks for model calibration, data assimilation and parameter estimation (e.g. Lardner et al. (1993), Canizares et al. (1998), Heemink et al. (2002), Lu and Zhang (2006), Zhang et al. (2011), Li et al. (2013), Chen et al. (2014)). Adjoint methods have previously been applied to the analysis of storm surge model sensitivity to wind stress (Wilson et al., 2013, Warder et al., 2019), and this paper represents an extension to these works.

Here, we apply a numerical coastal ocean model, *Thetis*, and its adjoint, to perform a storm surge sensitivity analysis with respect to multiple model inputs, namely the bottom friction coefficient, bathymetry and wind stress. We use the resulting sensitivities to gain physical insight into surge generation and propagation

in the North Sea, and to estimate and compare the uncertainty in surge model outputs arising from each of these inputs, and at different locations in the model domain. We first introduce the numerical model in section 2, and perform a brief model calibration in section 3. The adjoint approach to sensitivity analysis is described in section 4, and sensitivity analysis results are presented in section 5, using the extreme December 2013 storm surge event as a case study. The results of the sensitivity analysis are discussed in section 6, and conclusions are made in section 7.

## 2. Forward numerical model

Within this work, we model storm surges using *Thetis*, an unstructured-mesh finite element coastal ocean flow solver (Kärnä et al., 2018) implemented within the Firedrake finite element code generation framework (Rathgeber et al., 2016). We use Thetis in its two-dimensional configuration (Vouriot et al., 2019), which solves the shallow water equations (SWEs) in non-conservative form, given by

$$\begin{aligned} \frac{\partial \eta}{\partial t} + \nabla \cdot (H\mathbf{u}) &= 0, \\ \frac{\partial \mathbf{u}}{\partial t} + \mathbf{u} \cdot \nabla \mathbf{u} + \mathbf{F_C} + g\nabla\eta + \nabla\left(\frac{p_a}{\rho}\right) &= \frac{\boldsymbol{\tau}_s - \boldsymbol{\tau}_b}{\rho H} + \nabla \cdot (\nu_h(\nabla\mathbf{u} + \nabla\mathbf{u}^T)), \end{aligned} \tag{1}$$

where $\eta$ is the free surface height, $H$ is the water depth given by $H = \eta + h$ where $h$ is the bathymetry (measured positive downwards), $\mathbf{u}$ is the two-dimensional depth-averaged velocity vector, $\mathbf{F_C}$ is the Coriolis force, $g$ is the acceleration due to gravity, $\rho$ is the water density, $p_a$ is the atmospheric pressure at the free surface, $\boldsymbol{\tau}_b$ is the bottom stress due to friction with the sea bed, $\boldsymbol{\tau}_s$ is the surface stress due to wind, and $\nu_h$ is the kinematic viscosity. All variables are in SI units.

The bathymetry $h$ is taken from the GEBCO 2014 dataset, which has a resolution of 30 arc-seconds (or approximately 1 km), and is linearly interpolated onto the model mesh. A minimum depth of 10 m is then applied to avoid the need for wetting and drying, since we do not resolve the spatial scales of inundation within this study.

The bottom friction is parameterised via Manning's $n$ formulation, such that

$$\frac{\boldsymbol{\tau}_b}{\rho} = \frac{gn^2}{H^{\frac{1}{3}}}|\mathbf{u}|\mathbf{u}, \tag{2}$$

where $n$ is the Manning coefficient. We assume that the friction coefficient is spatially uniform and constant in time; this assumption is consistent with CS3X, the UK operational surge forecast model at the time of this event (Flowerdew et al., 2013). The Manning coefficient $n$ is determined by a preliminary calibration exercise, as described in section 3.

Storm surge forcing is included via $p_a$ and $\boldsymbol{\tau}_s$, which are the atmospheric pressure and surface stress due to wind, respectively. Within this work, we focus on the surge event of $5^{\text{th}}/6^{\text{th}}$ December 2013. Meteorological hindcast data for this event were provided by the National Oceanography Centre (personal communication 2018) at a spatial resolution of $1/9°$ latitude by $1/6°$ longitude, and a temporal resolution of 1 hour. This forcing data is linearly interpolated onto our model mesh and between timesteps for use within Thetis. We

use a Charnock parameterisation similar to Williams and Flather (2000) to relate $\boldsymbol{\tau}_s$ to the wind velocity, via the system of equations

$$\begin{aligned} \boldsymbol{\tau}_s &= \rho_{\text{air}} |\mathbf{W}_*| \mathbf{W}_*, \\ \mathbf{W} &= \mathbf{W}_* \frac{1}{\kappa} \log \frac{z}{z_0}, \\ z_0 &= \frac{\alpha |\mathbf{W}_*|^2}{g}, \end{aligned} \tag{3}$$

where $\rho_{\text{air}}$ is the density of air, $\mathbf{W}_*$ is the friction velocity, $\mathbf{W}$ the wind velocity at height $z$ above the free surface, assuming neutral atmospheric stratification, $\kappa$ is the von Kármán constant, taken to be 0.4, $z_0$ the surface roughness, and $\alpha$ the Charnock parameter, which we select via a calibration exercise as described in section 3. This Charnock parameter is assumed within this work to be spatially uniform and constant in time, neglecting any variation due to surface waves. This formulation is a common choice within storm surge modelling, and is consistent with that of the CS3X model (Williams and Flather, 2000, Flowerdew et al., 2010, 2013). The system of equations (3) is solved by a simple iterative method.

Tidal forcing is included within the model by applying a Dirichlet boundary condition for the free surface height on the open ocean boundaries, generated from eight harmonic constituents from the TPXO database (Egbert and Erofeeva, 2002) (M2, S2, N2, K2, Q1, O1, P1, K1). This boundary condition is further modified by a correction calculated from the inverse barometer effect, which is applied to approximate surge generated externally to the model domain.

The governing equations (1) are solved on an unstructured mesh using a $\mathrm{P}_1^{\mathrm{DG}}$-$\mathrm{P}_1^{\mathrm{DG}}$finite element pair, using approximate Riemann fluxes at element interfaces as described in Kärnä et al. (2018). This discretisation has been shown to be well suited for shallow water problems (Comblen et al., 2010). We use a Crank-Nicolson timestepping scheme with a timestep of 100 s. The mesh used within this work is shown in figure 1, in addition to a close-up of a key region of the domain. The mesh was generated using the Python package *qmesh* (version 1.0.1) (Avdis et al., 2018), which interfaces the mesh generator *Gmsh* (version 2.10.1) (Geuzaine and Remacle, 2009). The mesh uses the UTM31 coordinate system, and its resolution varies from 3 km at the coastline to 25 km in the open ocean, resulting in a total of 23,120 triangular elements. This coastline resolution is finer than that of the CS3X model (which has approximately 12 km resolution) (Flowerdew et al., 2013), while also benefitting from the alignment of element edges with the coastline, a key advantage of unstructured mesh methods (Pain et al., 2005). In open ocean regions, 25 km resolution is assumed to sufficiently capture the dynamics, since the tidal wavelength is $\mathcal{O}$(1000km). Each model run for this study was performed in parallel using 16 cores, on a machine with 124 GB memory, and each 30-day forward model run took a wall-clock time of approximately 7.5 hours.

## 3. Model calibration

We first calibrate the model with respect to the Manning coefficient $n$, based on a tide-only simulation. After a spin-up period of 10 days, the model is run in tide-only mode for one month, and a harmonic analysis

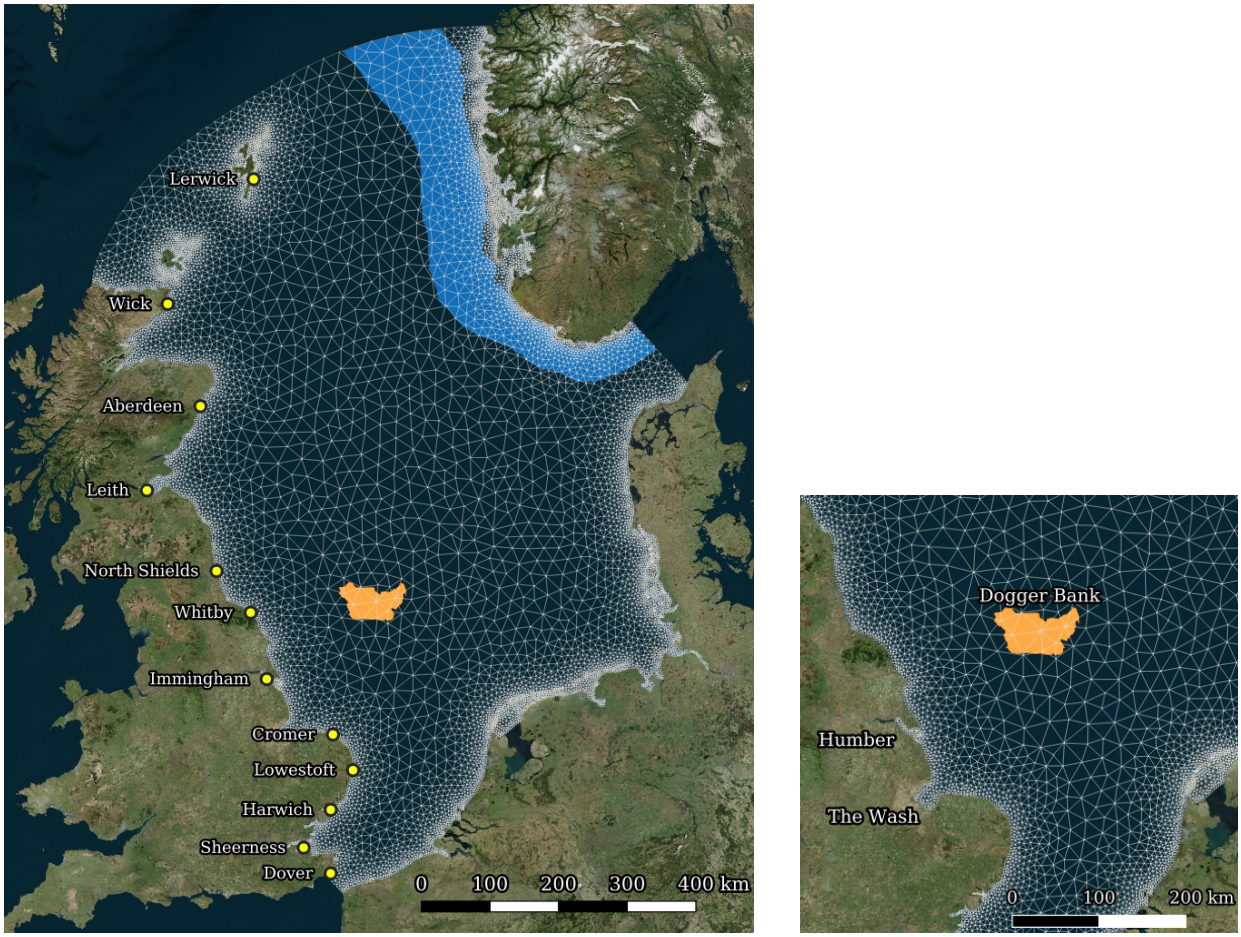


Figure 1: Left: Mesh used for all simulations within this work, consisting of 23,120 triangular elements. Tide gauge locations are shown for the east coast of the UK mainland. Two bathymetric features are highlighted for later reference: Dogger Bank (orange, extracted from 20 m bathymetry contour) and the Norwegian Trench (blue, extracted from 200 m bathymetry contour). Right: Close-up of a key region of the model domain, featuring the Humber, the Wash, and Dogger Bank.

performed at the 12 tide gauge stations within the model domain where quality controlled data is available from the British Oceanographic Data Centre (BODC) (see figure 1). We perform this harmonic analysis based on the same eight harmonic constituents as the tidal boundary condition, using the Python package *uptide* (Kramer et al., 2020). The model-observation error is computed via the combined root mean squared error (RMSE) of the amplitudes of the eight harmonic constituents $C$ by

$$\mathrm{RMSE} = \left( \frac{1}{8} \sum_{C} \frac{1}{12} \sum_{i=1}^{12} (A_{C,i} - \hat{A}_{C,i})^2 \right)^{\frac{1}{2}}, \tag{4}$$

where $A_{C,i}$ and $\hat{A}_{C,i}$ are the modelled and observed amplitudes of the harmonic constituent $C$ at tide gauge location $i$, respectively. The model was run as described above, for values of the Manning coefficient $n$ from 0.015 $\mathrm{s\,m^{-1/3}}$ to 0.04 $\mathrm{s\,m^{-1/3}}$ in steps of 0.0025 $\mathrm{s\,m^{-1/3}}$. The results are shown in figure 2; the smallest value for the RMSE was 5.7 cm, achieved with $n = 0.025$ $\mathrm{s\,m^{-1/3}}$. This value is used for the remainder of this paper. We note that the use of a spatially uniform value for the friction coefficient may restrict the

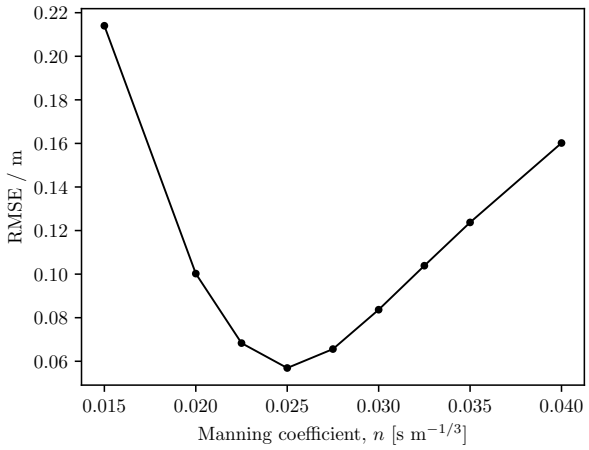


Figure 2: Calibration of the tidal model with respect to the Manning coefficient, $n$. The minimum RMSE is achieved using $n = 0.025$ s m$^{-1/3}$.

predictive capability of the model, but the RMSE attained with a uniform friction parameter is considered adequate, and more sophisticated model calibration is outside the scope of this work. It is assumed that the model sensitivities to the friction coefficient are not strongly dependent on the value of the coefficient itself.

In order to select an appropriate value for the Charnock parameter $\alpha$, the surge model was run for the December 2013 event using varying values of $\alpha$. For these simulations, the model is first spun up (in tide-only mode) for 10 days, prior to the wind and atmospheric pressure forcing terms being switched on approximately 10 days before the peak storm tide occurs. A comparison with observations for this event is made based on the modelled and observed surge residuals at the BODC tide gauge locations. As shown in figure 3, the surge residual is defined as the difference between the storm tide (i.e. the total sea surface height due to tidal and meteorological forcing) and the astronomical tide (i.e. the sea surface height which would be expected in the absence of meteorological forcing). For the tide gauge observations, the astronomical component is computed based on a harmonic analysis of long term tide gauge data, and this harmonic part is subtracted from the observed sea surface heights to obtain the residual. To compute the modelled residual, the model is simply run in both full surge (tidally and meteorologically forced) and tide-only modes, and the surface elevations subtracted. For the purposes of calibrating the Charnock parameter, the model-observation error is computed by a simple root mean squared error of the residual timeseries, over a two day period capturing the peak storm tide, at the eight BODC tide gauges within the domain at which the surge was significant, and which recorded a sufficiently complete timeseries surface elevation record during the event. The surge model was run as described, for values of the Charnock parameter $\alpha$ from 0.01 to 0.03, in steps of 0.002. The results are shown in figure 4; the smallest value for the residual RMSE was 15.9 cm, obtained using $\alpha = 0.028$, which is a value consistent with the literature (Williams and Flather, 2000, Brown and Wolf, 2009).

Using these calibrated parameters, a good agreement is obtained between modelled and observed surge

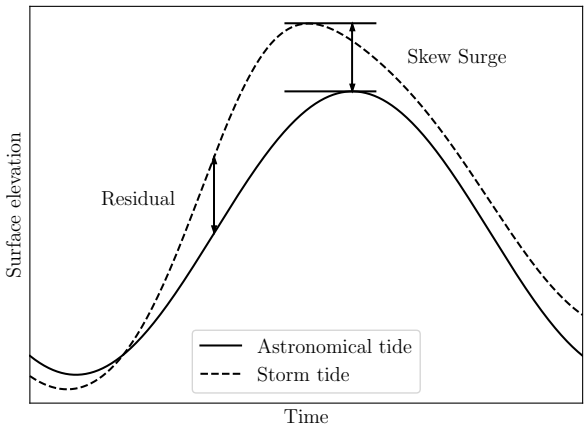


Figure 3: Schematic diagram of residual and skew surge definitions. The astronomical tide is the sea surface level which would be observed due to astronomical tidal forcing only. The storm tide is the sea surface level induced by the combination of the astronomical tide and meteorological conditions.

residuals for this event, as shown in figure 5 for the three tide gauge locations selected for the sensitivity analysis study. The smoothness of the model outputs compared with the observations arises from several factors, including the choice of mesh, discretisation (e.g. choice of finite element pair), timestepping, the representation within the model of the bathymetry and coastlines, and limitations in other model inputs. While adjustments to the model setup, e.g. the use of higher order mesh elements, might improve its predictive capability, the attained model-observation agreement is considered sufficient for the purposes of this study.

As an additional experiment, we tested alternative model meshes with (i) uniform 12 km resolution, and (ii) coastline resolution of 1.5 km and open-ocean resolution of 15 km. The residual RMSEs computed with these meshes were both within 1 cm of the RMSEs obtained using the final mesh we selected. This suggests that the selected mesh resolution does not limit our modelling accuracy, and that the model-observation misfit is dominated by other factors.

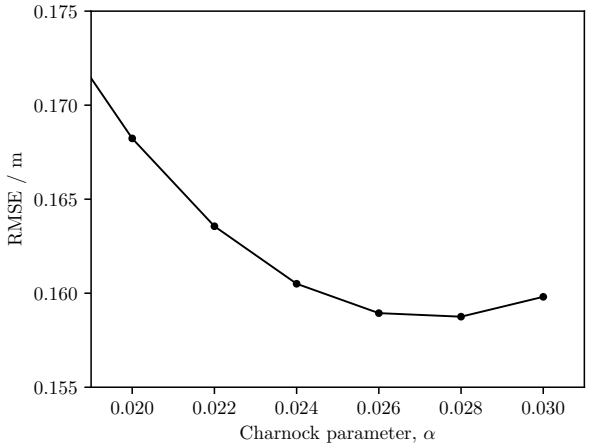


Figure 4: Calibration of the tidal model with respect to the Charnock parameter, $\alpha$. The minimum RMSE is achieved using $\alpha = 0.028$.

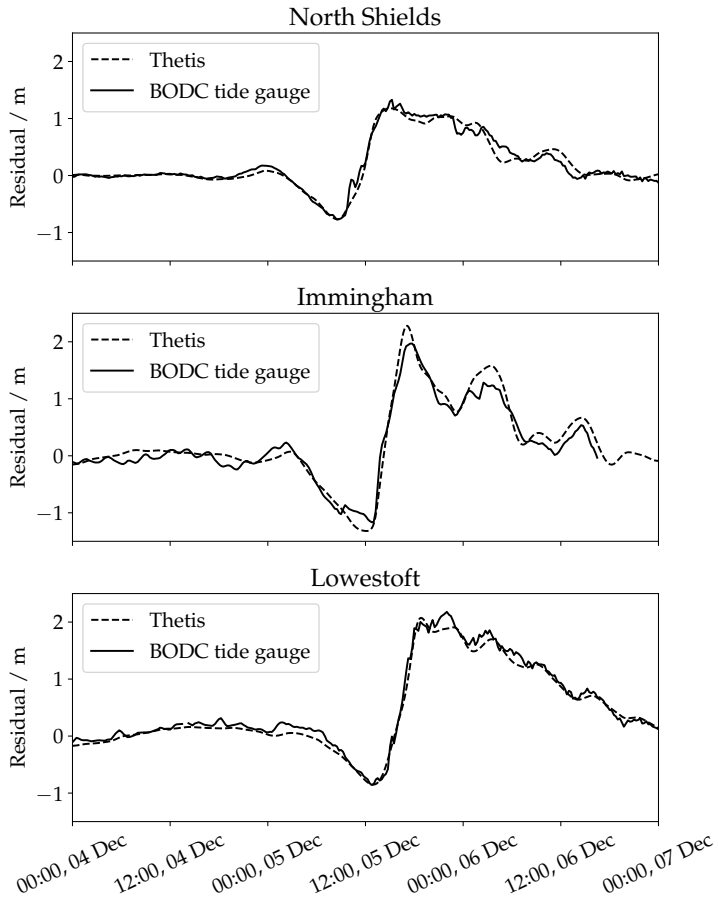


Figure 5: Comparison of modelled and observed surge residuals for the December 2013 event, at three selected tide gauge locations. The RMSEs between the modelled and observed residuals at at North Shields, Immingham and Lowestoft are 11.1, 19.6 and 11.3 cm, respectively.

## 4. Methods

### *4.1. The adjoint method*

In this section we briefly describe the adjoint method (based largely on Funke (2012)), and for further detail the reader is referred to similar works in the literature (e.g. Wilson et al. (2013), Verdy et al. (2014)) and previous studies utilising the adjoint mode of Thetis (e.g. Warder et al. (2019), Goss et al. (2020)).

For compactness, we write our system of PDEs in the general form

$$F(u, m) = 0, \tag{5}$$

where $F$ is the PDE operator (representing the shallow water equations (1)), $u$ is the model state variable (representing $\eta$ and $\mathbf{u}$) and $m$ represents the input parameters (bottom friction $n$, bathymetry $h$ and wind stress $\boldsymbol{\tau}_s$). A functional of interest is given by a scalar function $J(u)$. The purpose of the adjoint method is to efficiently compute the derivative of $J$ with respect to the input parameters $m$, i.e. $\frac{\mathrm{d}J}{\mathrm{d}m}$. It is straightforward to show that

$$\frac{\mathrm{d}J}{\mathrm{d}m} = -\frac{\partial J}{\partial u}\frac{\partial F}{\partial u}^{-1}\frac{\partial F}{\partial m}. \tag{6}$$

When solved in the forward time direction, this represents the so-called tangent linear approach to the evaluation of the gradient $\frac{\mathrm{d}J}{\mathrm{d}m}$. However, this approach is inefficient when there are a small number of functionals $J$, and a large number of parameters $m$, as is the case within this work. We therefore take the so-called adjoint approach. Equation (6) can be expressed as

$$\frac{\mathrm{d}J}{\mathrm{d}m} = -\lambda^*\frac{\partial F}{\partial m}, \tag{7}$$

where $\lambda$ is is the adjoint variable, defined as the solution to the adjoint equation

$$\frac{\partial F}{\partial u}^* \lambda = \frac{\partial J}{\partial u}^*, \tag{8}$$

where the asterisk denotes the adjoint operation (that is, the conjugate transpose). Note that this is a PDE; the adjoint variable $\lambda$ is space- and time-dependent, and the adjoint equation is solved in the reverse time direction (supposing that the functional $J$ depends only on the final state of the model variables, it is intuitive to interpret the right hand side of this equation as an initial condition, which is propagated backwards in time by the adjoint equation). Since the right-hand-side of equation (7) is a time-varying quantity, it represents the instantaneous influence of the parameter $m$ on the functional $J$. In the case where the inputs $m$ are not time-varying (i.e. for $m$ representing the bottom friction coefficient or bathymetry), the right-hand-side of this equation should be integrated over all time (although in practice here we integrate over a period of 10 days).

Note that the adjoint equation is always linear, and that the parameter $m$ does not appear in the equation. The computational cost of the numerical solution of the adjoint equation is therefore reasonably low, and does not depend on the number of parameters.


Figure 6: Selected target locations for sensitivity analysis. Three tide gauge locations are selected, along with an integrated measure along the indicated section of coastline.

For an application to numerical models, $u$ and $m$ in the above exposition should be interpreted as vectors representing the model state and input parameters, respectively. Specifically, $m$ corresponds to a vector of model inputs, whose elements correspond to the values of the input at each mesh node (and, in the case of the wind stress, at each time step). For models, such as Thetis, which are implemented within the Firedrake framework, the adjoint model can be generated algorithmically via the Python package *pyadjoint* (Mitusch et al., 2019, Farrell et al., 2013), removing the need to derive the adjoint equations by hand and implement their numerical solution.

For the model setup within this work, runs of Thetis in its adjoint mode were found to require approximately 2.4 times the wall-clock time of the forward mode. We emphasise that, since this computational cost is independent of the number of parameters $m$, the adjoint approach is especially powerful when used to calculate the derivative of a small number of model outputs with respect to a large number of inputs. Since the model inputs are defined at each mesh node (and at each time step in the case of wind stress), within this work the vector of input parameters $m$ contains $\mathcal{O}(10^6)$ elements. The adjoint method is therefore the only feasible approach to computing the sensitivity $\frac{\mathrm{d}J}{\mathrm{d}m}$.

### *4.2. Sensitivity analysis and uncertainty quantification*

Taking the December 2013 surge event, we use four definitions for the functional $J$. As indicated in figure 6, these correspond to the skew surges at three tide gauge locations (North Shields, Immingham and Lowestoft), and the mean skew surge along a section of coastline (measuring approximately 400 km, from Bridlington in the north to Great Yarmouth in the south, and including the Humber Estuary and the Wash). The skew surge is defined as the difference between the peak storm tide surface elevation and the peak astronomical (tidal) surface elevation, as shown in figure 3. The choice of skew surge as the selected

model output at each target location is motivated by Williams et al. (2016); the skew surge constitutes a more meaningful measure of surge severity than the surge residual. A functional defined as the skew surge at a location $\mathbf{x}_0$ can be broken down as

$$J_{\text{skew surge}} = J_{\text{peak storm tide}} - J_{\text{peak astronomical tide}}, \tag{9}$$

where

$$J_{\text{peak storm tide}} = \eta_{\text{storm tide}}(\mathbf{x}_0, t_{\text{peak storm tide}}), \tag{10}$$

and is computed with the model in full surge (tidally and meteorologically forced) mode, and

$$J_{\text{peak astronomical tide}} = \eta_{\text{tide only}}(\mathbf{x}_0, t_{\text{peak astronomical tide}}), \tag{11}$$

and is computed with the model in tide-only mode. The times $t_{\text{peak storm tide}}$ and $t_{\text{peak astronomical tide}}$ are determined from preliminary forward model runs. The sensitivity of the skew surge to each input $m$ is then defined as

$$\frac{\mathrm{d}J_{\text{skew surge}}}{\mathrm{d}m} = \frac{\mathrm{d}J_{\text{peak storm tide}}}{\mathrm{d}m} - \frac{\mathrm{d}J_{\text{peak astronomical tide}}}{\mathrm{d}m}. \tag{12}$$

A separate pair of forward and adjoint runs is required to evaluate the two terms on the right hand side of this expression; one with full (tide + meteorological) forcing, and one with tidal forcing only. However, when the model input $m$ is taken as the wind stress, the second term on the right hand side is zero since, by definition, the tidally induced peak surface height is independent of the meteorological forcing.

Using the adjoint model, we evaluate equation (12) for three model input fields $m$, namely the bottom friction coefficient $n$, bathymetry $h$ and wind stress $\boldsymbol{\tau}_s$. We note that the atmospheric pressure is also an important model input for surge modelling; however, for this event its overall contribution to the modelled storm tide is around 10%, and we therefore choose to focus on wind stress as the primary surge-generating input. The bottom friction coefficient and bathymetry are both scalar fields which are constant with respect to time, and the sensitivity pattern we compute with respect to these inputs is therefore only spatially varying. When computing the model sensitivities with respect to these inputs, we perform the adjoint model run over a period of approximately 10 days prior to the peak storm tide. This 10-day period was found to be sufficient, with longer periods having negligible effect on the computed sensitivities. Wind stress is a vector field which varies in both space and time, and the sensitivity of modelled skew surges with respect to wind stress is therefore also a spatially and temporally varying vector field. The wind stress sensitivity results presented here are computed from adjoint model runs spanning two days prior to the peak storm tide. The sensitivity of the modelled skew surge to the wind stress prior to this period was found to be small.

The spatial (and temporal) patterns of sensitivity to each model input reveal insights into the modelled system, but the sensitivities to different inputs cannot be directly compared, since they have incommensurable units. However, if we consider a perturbation in the input, $\Delta m$, and perform a convolution with the sensitivity, we can obtain an estimate of the resulting perturbation in the skew surge, $\Delta J$, via

$$\Delta J \approx \int\int\int \frac{\mathrm{d}J}{\mathrm{d}m}(x, y; t) \cdot \Delta m \;\; \mathrm{d}x \, \mathrm{d}y \, \mathrm{d}t. \tag{13}$$

This $\Delta J$ can be directly compared for different inputs $m$, and we are thus able to compare the first-order influence of each input parameter on the modelled skew surges, based on simple estimates for $\Delta m$. Note that this is equivalent to performing a first-order Taylor expansion with respect to the input $m$, and that the resulting $\Delta J$ may be positive or negative for a given perturbation $\Delta m$. The use of this equation is valid as long as the perturbations fall within the linear response regime of the model. While the inclusion of higher order terms would extend the validity of a Taylor expansion approach beyond the range of linear response, the calculation of higher order derivatives via adjoint methods is beyond the scope of this work.

For the purpose of uncertainty quantification within this paper, only spatially uniform $\Delta m$ are considered. This is an approximation to the true uncertainty, since real errors in the model inputs are likely to vary spatially. However, in the absence of information about the spatial correlation of the input errors (the estimation of which is beyond the scope of this work), $\Delta J$ is taken as a simple estimate of the model output uncertainty.

## 5. Results

### *5.1. Sensitivity to bottom friction coefficient*

The fields of sensitivity to bottom friction coefficient for each target location are shown in figure 7. The greatest sensitivity magnitudes are found within relatively small regions in the vicinity of each target location. The sensitivity of the skew surge at North Shields exhibits the smallest sensitivity magnitudes, due to its position on an exposed section of coastline; the propagation of the surge as a coastally trapped wave is not strongly affected by local features, and the local value of the bottom friction coefficient therefore has only a weak effect on the skew surge at the North Shields tide gauge. The sensitivity of the skew surge at Immingham exhibits the greatest magnitudes, particularly in and around the Humber Estuary and the Wash. The dynamics of the surge propagation around this region are complex, and the waters here are particularly shallow; the $1/H$ proportionality in the wind stress and bottom stress terms of the governing equations (1) therefore increases the model's sensitivity to bottom friction, as well as to bathymetry and wind stress, in shallow waters. This high sensitivity to the friction coefficient in the region of the Humber Estuary and the Wash is also evident for the skew surge at Lowestoft, suggesting that the interaction between the surge and this region of coastline has a lasting effect on the surge as it travels further south.

Common to the sensitivity patterns for all target locations is the pattern in the far-field, i.e. in the north of the domain. This is because any effect of the bottom friction on the surge in the north of the domain is propagated with the surge as it travels south as a coastally trapped wave, and therefore has the same effect on the skew surge at all target locations.

In order to estimate the total impact of an uncertain bottom friction coefficient on model outputs via equation (13), we first estimate the uncertainty in the bottom friction coefficient ($\Delta m$ in equation (13)). Based on typical values for the Manning coefficient (Arcement and Schneider, 1989) for the types of sediment found in the North Sea (Digimap, b), we assume an uncertainty in the Manning coefficient of $0.005\ \mathrm{s\,m^{-1/3}}$.

Using equation (13) to convolve a uniform perturbation of 0.005 $\mathrm{s\,m^{-1/3}}$ with the adjoint sensitivities shown in figure 7, we obtain skew surge perturbations of -8.1 cm at North Shields, -17.3 cm at Immingham and -16.1 cm at Lowestoft, with the minus signs indicating that increases in friction would induce reductions in skew surge, due to the extraction of energy from the surge. The uncertainty in the mean skew surge along the coastline section, estimated by the same method, is -19.9 cm; this is of similar magnitude to the estimated uncertainties at Immingham (which is within the coastline section) and Lowestoft (just to the south of the coastline section).

### *5.2. Sensitivity to bathymetry*

The sensitivities of modelled skew surges to bathymetry are shown in figure 8. The observed spatial patterns share similar features to those of the sensitivity to bottom friction coefficient of figure 7. We find the greatest magnitudes of sensitivity within localised regions around each target location, and in particular we find that these localised sensitivities share similar spatial patterns with those observed for bottom friction, but with opposite signs. In the north of the domain, we again find that the observed patterns of bathymetry sensitivity are similar for all target locations, due to the propagation of the surge as a coastally trapped wave from north to south; any influence of the bathymetry on the surge in the north of the domain is propagated south with the surge and impacts all subsequent observation locations.

To estimate the impact of this sensitivity on model outputs, we again start by estimating the uncertainty in the bathymetry itself. For this, we compute the root mean square (RMS) difference between two bathymetric datasets. We compare the GEBCO bathymetry dataset used within the model with data from Digimap (Digimap, a), which is available at higher resolution than GEBCO, but does not cover the entire model domain. In the region of our model domain in which both GEBCO and Digimap datasets are available, the RMS difference between the two is 2.7 m. Convolving a uniform 2.7 m bathymetry perturbation with the adjoint-computed bathymetry sensitivities via equation (13) produces perturbations of -2.3 cm, 6.7 cm and -4.8 cm in the skew surges at North Shields, Immingham and Lowestoft, respectively, and -3.7 cm in the mean skew surge along the coastline section. The minus signs for North Shields, Lowestoft and the coastline section indicate that an increase in bathymetry (i.e. an increase in water depth) induces a decrease in the skew surge, with the opposite being the case at Immingham.

One feature common to the bathymetry sensitivity for Immingham, Lowestoft and the coastline section is the region of positive sensitivity coinciding with Dogger Bank, to the north-east of the Humber Estuary (see figure 1). The depth of this sand bank is around 20 m, with depths in excess of 60 m immediately north of the bank. The positive sign of the bathymetry sensitivity in this region indicates that an increase in bathymetry (i.e. the removal of the bank) would produce an increase in the skew surges at Immingham, Lowestoft and the coastline section, and therefore that the bank protects the coastline to its south from the surge.

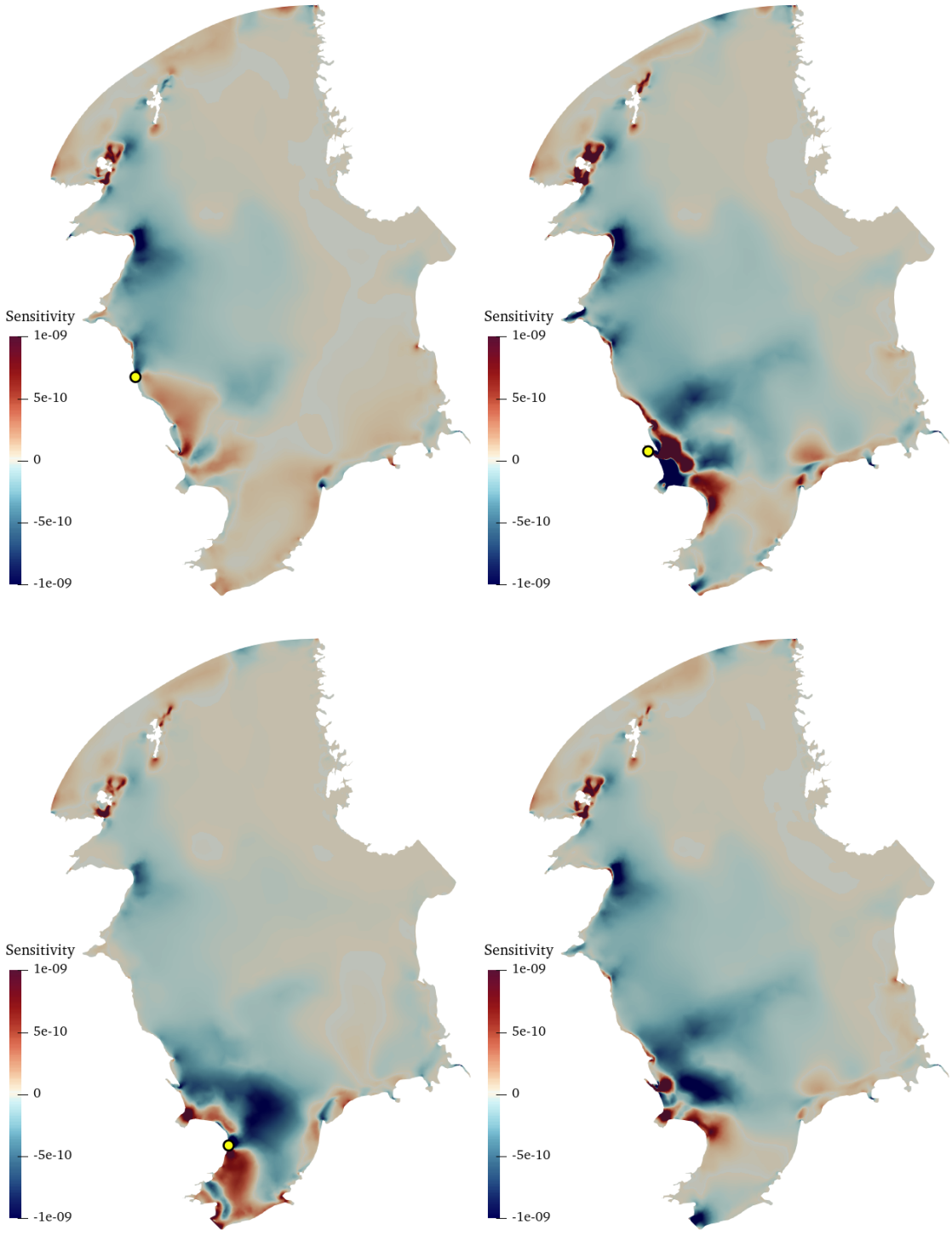


Figure 7: Sensitivity of modelled skew surges to the bottom friction coefficient. Units: $\mathrm{m\,s^{-1}\,m^{1/3}\,m^{-2}}$ (metres of surge, per unit Manning coefficient, per unit area). The relevant tide gauge locations are indicated by yellow circles. Top left: North Shields. Top right: Immingham. Bottom left: Lowestoft. Bottom right: mean along coastline section. The greatest sensitivity magnitudes are local to each location, and all locations exhibit similar patterns of sensitivity to bottom friction coefficient in the north of the domain.

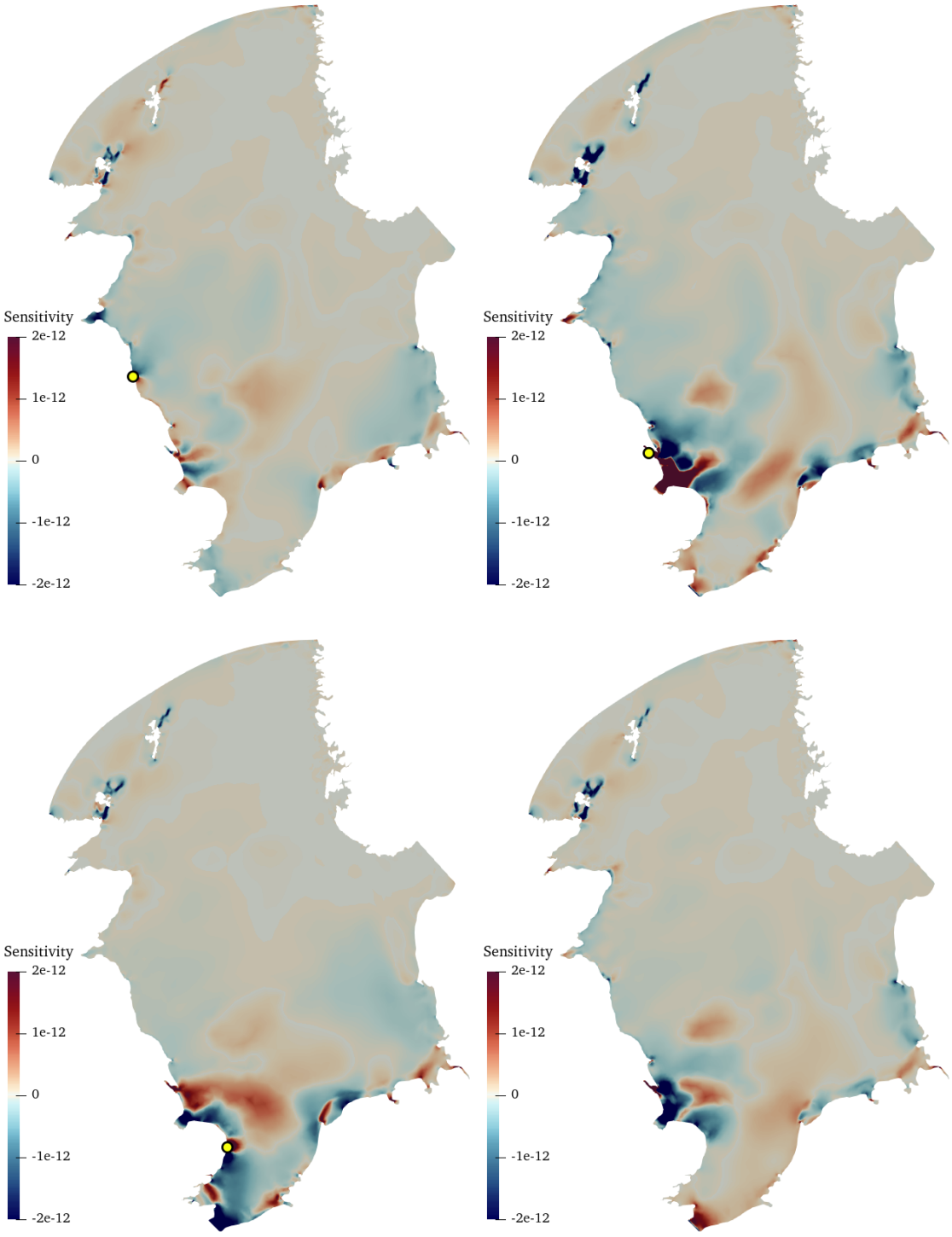


Figure 8: Sensitivity of modelled skew surges to the bathymetry. Units: $\mathrm{m\,m^{-1}\,m^{-2}}$ (metres of surge, per metre of bathymetry, per unit area). The relevant tide gauge locations are indicated by yellow circles. Top left: North Shields. Top right: Immingham. Bottom left: Lowestoft. Bottom right: mean along coastline section. The greatest magnitudes are found in the vicinity of the target locations, and the patterns in the north of the domain are similar for all target locations.

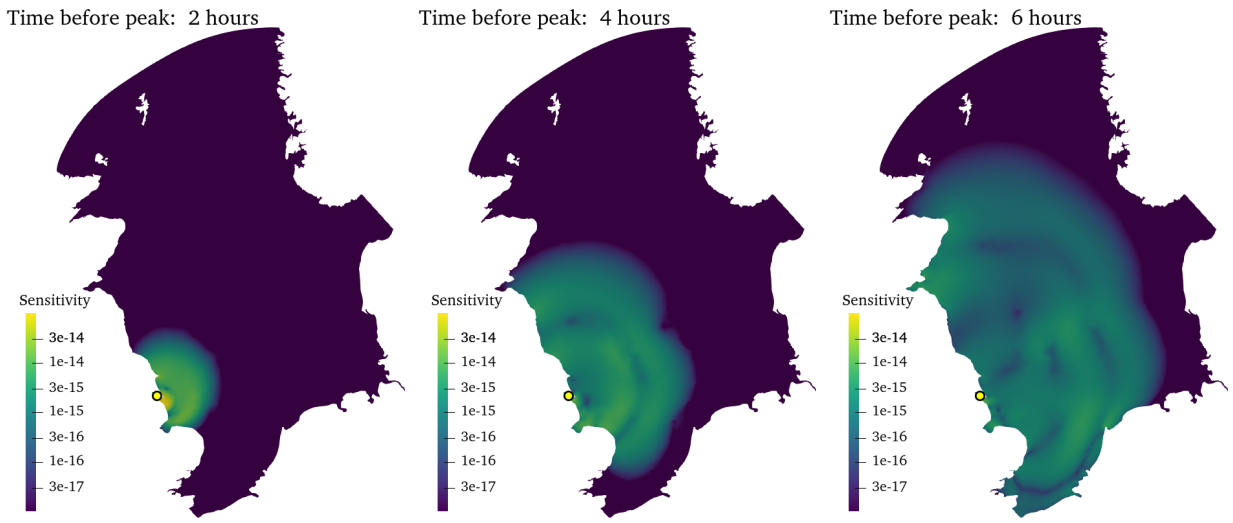


Figure 9: Snapshots of the magnitude of the sensitivity of the skew surge at Immingham to wind stress at various times prior to the peak storm tide, as labelled. Units: $\mathrm{m\,Pa^{-1}\,m^{-2}\,s^{-1}}$ (metres of surge, per Pa wind stress, per unit area, per second). The yellow circle indicates the Immingham tide gauge location. The region of influence of the wind stress on the skew surge increases with lead time, due to the propagation of perturbations being limited by the shallow water wave speed.

### *5.3. Sensitivity to wind stress*

Wind stress and atmospheric pressure are responsible for surge generation, and the sensitivity of a surge model to these inputs therefore has the potential to provide physical insight into the surge generation mechanism. In an operational scenario, the meteorological inputs also carry high uncertainty, and understanding model sensitivity to these inputs is therefore essential to the interpretation of surge forecasts. Since the wind stress varies in space and time, so too do the sensitivities of modelled skew surges with respect to the wind stress. Considering a model output functional $J$ corresponding to the peak storm tide elevation at a single location, the region of influence of the wind stress on $J$ will expand as lead time increases, as shown in figure 9. This is due to the fact that the propagation of perturbations caused by wind stress is limited to the shallow water wave speed. For this reason, the sensitivity to wind stress can be considered as a shallow water wave propagating backwards in time, originating at the point at which the functional is defined. This has been explored in detail previously (Wilson et al., 2013), and can be further confirmed by an analytic approach (Warder et al., 2019).

In order to make progress comparing the wind stress sensitivities of skew surges at different locations, we can integrate the wind stress sensitivity field with respect to time to obtain an overall spatial pattern. These time-integrated sensitivities are shown in figure 10 for each target location. Similarly to the sensitivities to bottom friction coefficient and bathymetry, there are regions of high sensitivity magnitude in the vicinity of each target location, where local winds shortly before the peak storm tide occurs have a significant effect on the value of the peak sea surface height (and hence skew surge). All four target locations exhibit similar patterns of sensitivity to wind stress in the north of the domain, but differ more in the south, because any

perturbations induced by wind stress in the north of the domain affect the coastally trapped wave which then impacts all target locations as it travels south.

The magnitudes of wind stress sensitivity are generally greater in the west of the domain. This is due to the southerly propagation of the surge along the western coastal boundary of the model domain (the east coast of the UK); winds in the east of the domain therefore have relatively little effect on the surge impacting the UK locations considered within this study. In particular, sensitivity magnitudes over the Norwegian Trench are very small. This is likely to be due to the very large depths in this region, and the $1/H$ proportionality in the wind stress term in the governing equations (1).

It is not possible to make a generally applicable estimate of the uncertainty associated with wind stress, since in a forecast scenario this depends strongly on the forecast lead time, and the nature of the surge event. To make a simple comparison between the overall wind stress contribution to uncertainty for each target location, we take uniform (in both space and time) wind stress perturbations of 0.1 Pa in each of the $x$- and $y$-directions, and convolve these with the adjoint-derived sensitivities via equation (13). The output perturbations calculated for the 0.1 Pa wind stress perturbations in the positive $x$-direction are 0.5, -1.2, 3.0 and 0.3 cm for North Shields, Immingham, Lowestoft and the coastline section, respectively. The corresponding output perturbations for wind stress perturbations in the positive $y$-direction are -5.5, -8.0, -10.8 and -9.1 cm, respectively. Firstly, these results show that modelled skew surges can be significantly increased by wind stress perturbations in the negative $y$-direction (north to south), while wind stress perturbations in the $x$-direction (east-west) have a smaller effect which is more variable across the target locations. Secondly, the overall sensitivities to wind stress perturbations show an increasing trend for gauges further south, due to the southward propagation of the surge and the corresponding accumulation of influence of wind stress.

## 6. Discussion

### *6.1. Comparison of uncertainties*

In section 5 we used the adjoint model to explore the spatial patterns of storm surge model sensitivity to its uncertain inputs. In the cases of bottom friction coefficient and bathymetry, we have estimated uncertainties in each model input and, through convolution with the model sensitivity, estimated the resulting uncertainties in the model outputs, namely the skew surges at selected coastal target locations. In contrast to the raw sensitivities, these estimated output uncertainties can be directly compared. A summary of these estimated uncertainties is shown in table 1. We make three key observations:

(i) Estimated uncertainties due to bottom friction are of greater magnitude than those due to bathymetry. However, it should be noted that we have made very simple estimates of input uncertainties, and for a well-calibrated model these uncertainties would likely be significantly reduced. This is particularly the case for the bottom friction, and these results highlight the importance of achieving a tight constraint on the bottom friction coefficient through model calibration methods.

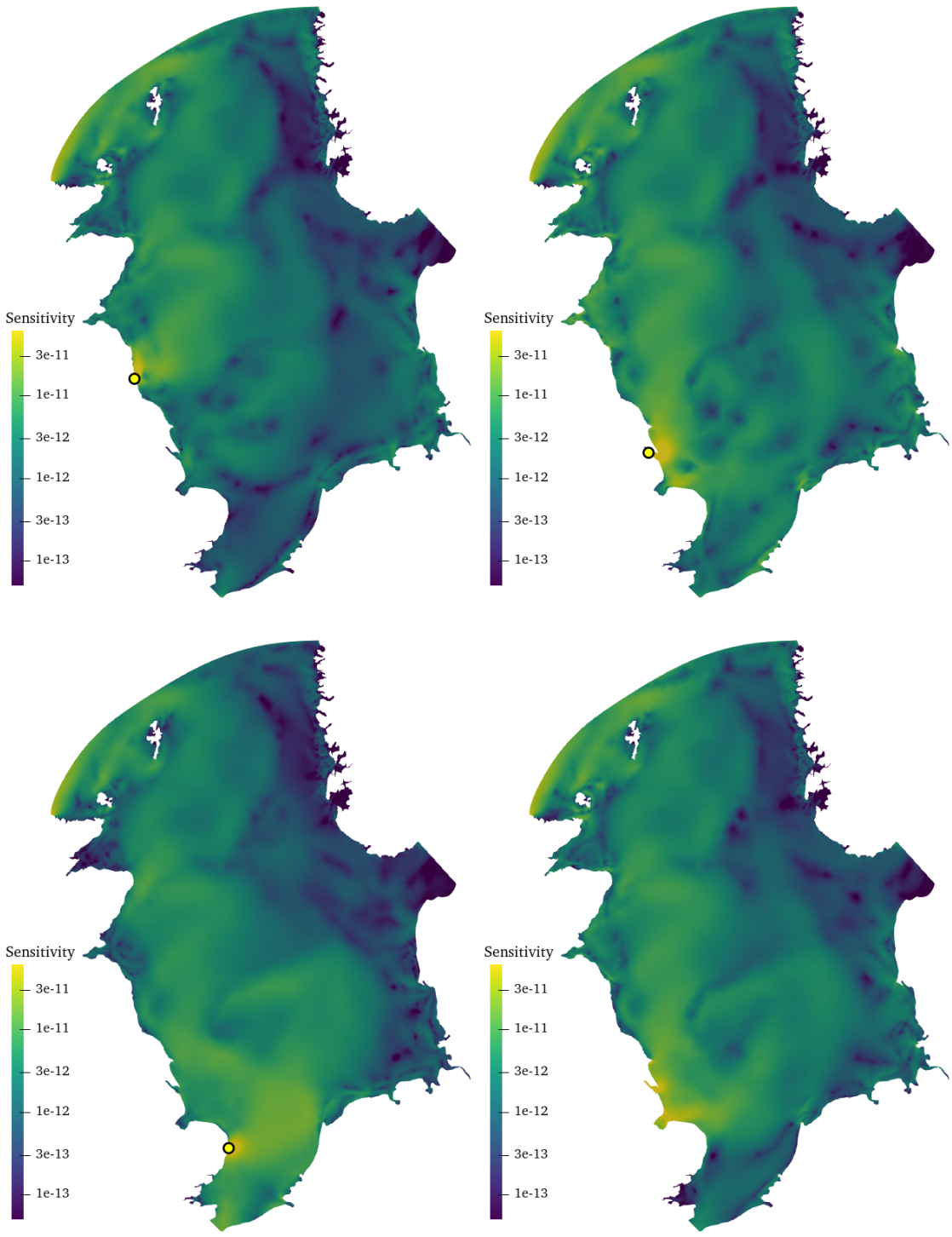


Figure 10: The magnitude of the time-integrated sensitivity of modelled skew surges to wind stress. Units: $\mathrm{m\,Pa^{-1}\,m^{-2}}$ (metres of surge, per Pa wind stress, per unit area). The relevant tide gauge locations are indicated by yellow circles. Top left: North Shields. Top right: Immingham. Bottom left: Lowestoft. Bottom right: coastline section. The greatest magnitudes are local to each target location, and there is a similar pattern in the north of the domain for all target locations.

| | North Shields | Immingham | Lowestoft | Coastline section |
|---|---|---|---|---|
| Bottom friction coefficient ($\pm$ 0.005 $\mathrm{s\,m^{-1/3}}$) | $\mp$ 8.1 cm | $\mp$ 17.3 cm | $\mp$ 16.1 cm | $\mp$ 19.9 cm |
| Bathymetry ($\pm$ 2.7 m) | $\mp$ 2.3 cm | $\pm$ 6.7 cm | $\mp$ 4.8 cm | $\mp$ 3.7 cm |

Table 1: Summary of estimated skew surge uncertainties due to bottom friction coefficient and bathymetry, calculated from adjoint-derived sensitivities and estimated input uncertainties. In almost all cases, the response of the skew surge to positive perturbations in the inputs is a decrease in the skew surge, as indicated by the $\mp$ signs in the uncertainties, i.e. deeper water or increased friction results in decreased skew surges. The effect of bathymetry at Immingham is the exception, where a positive bathymetry perturbation (deeper water) results in increased skew surge.

(ii) The uncertainty contributed by the bottom friction is of smaller magnitude for the northernmost target location (North Shields) than for the locations further south, which all exhibit similar magnitudes. This pattern is explained by the accumulation of uncertainty over the propagation path of the surge along the east coast of the UK; bottom friction acts to remove energy from the surge, and this effect is therefore cumulative along the path of the surge from north to south.

(iii) In contrast, the overall contribution of uncertain bathymetry exhibits a more variable pattern across the domain, suggesting that the effect of the bathymetry on the skew surge arises through a variety of mechanisms. The similarity (with opposite signs) between the localised spatial patterns of sensitivity to bottom friction coefficient and bathymetry (figures 7 and 8) suggests that a proportion of the sensitivity to bathymetry in these regions arises from the bottom friction term of the governing equations, which is inversely proportional to the water depth. However, given the contrasting patterns of estimated uncertainty due to each input summarised in table 1, it is clear that the sensitivity to bathymetry is more complex, and must also derive significant contributions from the other terms of the governing equations (1) in which the bathymetry $h$ appears, i.e. the wind stress and surface elevation advection terms.

Regarding the overall sensitivity to wind stress, our results indicate that modelled skew surges exhibit positive sensitivity to wind stress perturbations in the negative $y$-direction, i.e. that wind stress perturbations aligned with the southerly propagation of the surge act to increase the peak storm tide. Since the uncertainty in the wind stress depends strongly on the forecast lead time, a direct comparison between uncertainty due to bottom friction, bathymetry and wind stress is not possible. However, we know from ensemble forecasts for this event that the uncertainty due to meteorological inputs was on the order of 1 m at a forecast lead time of 24 hours; this is far greater than the uncertainties due to bottom friction and bathymetry estimated here. The quantitative results of this study are therefore consistent with the perceived limitations of the operational model at the time, namely that storm surge forecast model performance is limited by the accuracy of the meteorological forecast providing the wind stress (and atmospheric pressure).

### *6.2. Implications and limitations*

The results of an adjoint sensitivity analysis as performed within this study are highly relevant at the interface between models and observations. The spatial pattern of sensitivity to bottom friction coefficient could, for example, be used to inform the intelligent application of a spatially varying bottom friction coefficient, for the purposes of more sophisticated model calibration. For example, a choice of length scale of variation in bottom friction coefficient could be made based on the spatial variability of the model sensitivity, since variations on smaller length scales would not be constrained by observations. Similarly, the relatively localised impact of uncertain bathymetry shown here suggests that bathymetric surveys, particularly in regions prone to morphological change, could be valuable in reducing uncertainty in storm surge forecasts. This bathymetric sensitivity also suggests that the impact of imposing a minimum water depth for model stability purposes, as we have done within this study, should be carefully considered. Finally, the observed patterns of sensitivity to wind stress could be used to inform efforts to enhance meteorological models, by identifying regions in which uncertainty in wind stress has the greatest impact on overall surge uncertainty.

In addition to assisting in analysing surge model performance, the adjoint-based sensitivity analysis performed within this work is capable of providing physical insight into surge generation and propagation. The skew surges at Immingham, Lowestoft and the coastline section all show a positive gradient with respect to the bathymetry over Dogger Bank, to the north-east of the Humber Estuary; this is visible in figure 8. This reveals the protective effect of this bank for the south-east coast of the UK, against this storm surge event. Similarly, the sensitivity to wind stress of figure 10 shows very low sensitivity over the Norwegian Trench, due to the deep water in this region. Features such as these are simple to interpret within the physics contained in the governing equations. However, quantifying the impact of these features on the generation and propagation of the surge is non-trivial, but is achieved at relatively low computational cost by the adjoint techniques employed here.

The sensitivity analysis approach we have taken here consists of computing gradients of model outputs with respect to model inputs. This facilitates a linearisation of the model with respect to the inputs considered, i.e. the use of a Taylor expansion as a substitute for the full forward model, via equation (13). This expansion is only valid for sufficiently small perturbations of the model inputs, but could be used, for example, to estimate an arbitrarily large ensemble of model outputs at the computational cost of only one forward and one adjoint model run (since the cost of evaluating the Taylor expansion is negligible compared to running the full numerical model). Since the adjoint model used here requires approximately 2.4 times the computation time of the forward model, this constitutes a highly efficient approach. This is of particular interest for uncertain wind stress, where operational uncertainty quantification is typically carried out using ensemble methods. However, the viability of the adjoint-based approach as a substitute for an ensemble method is limited by two key factors. Firstly, the range of perturbations in the ensemble may exceed the linear response regime of the model, and secondly, the adjoint model must be computed separately for every model output of interest. An ensemble forecast or hazard assessment over a large spatial scale is therefore not

feasible using adjoint methods alone. However, as we have shown here, an adjoint-based sensitivity analysis can provide information complementary to ensemble methods; for a given event, the adjoint in conjunction with an ensemble method could provide a more complete analysis of the potential inundation consequences for flood risk assessment purposes than ensemble methods alone.

We note a number of avenues for further work. In order to gain estimates of model uncertainties due to each input, we have propagated uniform perturbations through the model, via the adjoint-derived sensitivities. The use of spatially varying input perturbations would require an estimate of the spatial correlation of errors in the model inputs, which was beyond the scope of this work but may be considered in future. We also note that the model output perturbations could have been computed from forward model runs alone. However, the use of the Taylor expansion approach via the adjoint-derived sensitivities is a demonstration of the efficiency of the adjoint method for propagating input perturbations through the numerical model at low computational cost (once the adjoint model has been run), and is central to the efficient propagation of large ensembles through the model, as described above.

We further note a number of modelling choices we have made within this study, whose influence could be investigated in future work. Firstly, we have not included waves within our numerical model, even though wave effects may have contributed 40 cm to the surge for this event (Staneva et al., 2017). In particular, we have used a constant Charnock parameter to capture the atmosphere-ocean coupling, whereas this parameter is thought to depend on wave age (Drennan et al., 2005, Brown and Wolf, 2009). However, our modelling assumptions are consistent with the CS3X model used operationally at the time of the case study event, and our model performance (based on the RMSEs of modelled surge residuals) is comparable with CS3X. Furthermore, the model sensitivity to the wind stress is independent of the wind stress parameterisation itself (i.e. we are not computing sensitivity with respect to the wind velocity), and we therefore assume that our results are not significantly impacted by our choice to neglect waves. Similarly, we have not included near-shore effects such as wave setup, which may have influenced the observed storm tide. We leave the inclusion of these effects, and the study of their subsequent impact on model sensitivities, to future work. Secondly, we have used a uniform value for the friction coefficient within the model, although the spatial variation of this parameter can have a significant impact on modelled surges (as highlighted within this work). However, additional forward model runs revealed that, for a perturbation in the Manning coefficient of $0.001\ \mathrm{s\,m^{-1/3}}$, nonlinear contributions to the resulting storm tide perturbation were around 2%. We therefore assume that nonlinear effects are sufficiently small that the computed sensitivities to the friction coefficient do not depend strongly on its input value. Finally, the use of a minimum water depth, to avoid the need to include wetting and drying within the model, may inhibit the predictive capability of the model, and is likely to have influenced the model calibration. Due to the model resolution and bathymetry dataset used, the application of a 10 m minimum depth only impacts upon a small fraction of the UK east coast, although parts of the Humber Estuary and the Wash were affected, thus potentially impacting the model results at Immingham and the coastline section, and possibly Lowestoft. The results of this work, which show high sensitivity

to bathymetry in localised regions around each target location, suggest that the bathymetry modification in shallow regions may be important, and therefore that accurate surge modelling requires small values of imposed minimum depths, or ideally the inclusion of wetting and drying, even if inundation modelling is not the focus. The use of a minimum depth within this study may have led to an underestimation of model sensitivities to all uncertain inputs in these localised shallow regions, but an investigation into this influence is beyond the scope of this study.

## 7. Conclusions

In this work, we have applied adjoint methods to perform sensitivity analysis and uncertainty quantification for a storm surge model, in particular comparing the sensitivity of the modelled skew surge, at different locations across the domain, to three different model inputs, namely the bottom friction coefficient, bathymetry and wind stress. Based on the results of this work, conclusions can be drawn based on both the underlying sensitivity patterns revealed, and also the resulting estimates of model uncertainty due to each of the model inputs.

The underlying patterns of skew surge sensitivity to all model inputs considered exhibit high spatial variability, with high sensitivity magnitudes in localised regions around each target location. However, we also find that the sensitivity to model inputs in the north of the domain is similar for all target locations; i.e. perturbations in bottom friction, bathymetry or wind stress in the north of the domain have a similar impact on all target locations. This is consistent with the storm surge propagating south as a coastally trapped wave along the east coast of the UK, since any effect of the model inputs on the surge in the north of the domain will travel south with the wave and impact all locations in its path. The spatial variability of sensitivity to each input has potentially broad implications, such as the application of a spatially varying bottom friction coefficient, the commissioning of new bathymetric surveys in regions where high sensitivity aligns with high bathymetry uncertainty, or to provide feedback informing improvements of the meteorological models providing the wind stress and atmospheric pressure forcing for surge models.

Physical insight can also be gained from the patterns of surge sensitivity. For example, we see in the sensitivity to bathymetry that locations on the UK coast towards the south of the domain are protected from the surge by Dogger Bank, a large sand bank around 200 km off the UK coast. We also find that sensitivity to wind stress is particularly low over the Norwegian Trench, due to the very deep water. These are good examples of how adjoint methods can be used to gain physical insight, and form a valuable tool for analysing the impact of a storm surge event.

Using the adjoint-derived sensitivities to estimate the uncertainty in a skew surge model prediction due to typical uncertainty in each input, we find that an uncertainty of 0.005 $\mathrm{s\,m^{-1/3}}$ in the Manning coefficient produces uncertainty of around 15 cm in the modelled skew surge, highlighting the importance of model calibration in constraining this uncertainty. Similarly, we estimate that an uncertainty of 2.7 m in the bathymetry produces uncertainty of around 5 cm in the modelled skew surge. The contribution from

uncertain meteorological inputs can be on the order of 1 m in an operational forecast scenario, far exceeding the uncertainty due to bottom friction or bathymetry, and ensemble methods remain the most practical approach to uncertainty quantification in a forecast scenario. However, we have shown here how an adjoint-based sensitivity analysis provides complementary information to an ensemble approach, providing detailed spatial and temporal information about how input uncertainty is mapped onto outputs.

## Acknowledgements

This work was funded by the EPSRC Centre for Doctoral Training in Fluid Dynamics across Scales (Grant EP/L016230/1). MDP would additionally like to acknowledge EPSRC support under Grant EP/R029423/1. We thank Jane Williams of the National Oceanography Centre for her contribution of hindcast data. We also acknowledge the Research Computing Service at Imperial College London for access to computing resources. This study uses data from the National Tidal and Sea Level Facility, provided by the British Oceanographic Data Centre and funded by the Environment Agency.

## References

G. J. Arcement and V. R. Schneider. Guide for Selecting Manning's Roughness Coefficients for Natural Channels and Flood Plains. Technical report, 1989.

ASC. Managing climate risks to well-being and the economy. Adaptation Sub-Committee. Committee on Climate Change. Progress report 2014., 2014.

A. Avdis, A. S. Candy, J. Hill, S. C. Kramer, and M. D. Piggott. Efficient unstructured mesh generation for marine renewable energy applications. *Renewable Energy*, 116:842–856, 2018. ISSN 0960-1481. doi: https://doi.org/10.1016/j.renene.2017.09.058. URL http://www.sciencedirect.com/science/article/pii/S0960148117309205.

J. M. Brown and J. Wolf. Coupled wave and surge modelling for the eastern Irish Sea and implications for model wind-stress. *Continental Shelf Research*, 29(10):1329–1342, may 2009. ISSN 0278-4343. doi: 10.1016/J.CSR.2009.03.004. URL https://www.sciencedirect.com/science/article/pii/S0278434309001010.

R. Canizares, A. W. Heemink, and H. J. Vested. Application of advanced data assimilation methods for the initialisation of storm surge models. *Journal of Hydraulic Research*, 36(4):655–674, 1998. doi: 10.1080/00221689809498614. URL https://doi.org/10.1080/00221689809498614.

H. Chen, A. Cao, J. Zhang, C. Miao, and X. Lv. Estimation of spatially varying open boundary conditions for a numerical internal tidal model with adjoint method. *Mathematics and Computers in Simulation*, 97:14–38, mar 2014. ISSN 0378-4754. doi: 10.1016/J.MATCOM.2013.08.005. URL https://www.sciencedirect.com/science/article/pii/S0378475413002000.

R. Comblen, J. Lambrechts, J.-F. Remacle, and V. Legat. Practical evaluation of five partly discontinuous finite element pairs for the non-conservative shallow water equations. *International Journal for Numerical Methods in Fluids*, 63(6):701–724, 2010.

Digimap. Marine Themes Digital Elevation Model 6 Arc Second [ASC geospatial data], Scale 1:250000, Tiles: 2062000000, 2060010060, 2060010040, 2060010020, 2060000000, 2058010080, 2058010060, 2058010040, 2058010020, 2058000000, 2056010080, 2056010060, 2056010040, 2056010020, 2056000020, 2056000000, 2054010080, 2054010060, 2054010040, 2054010020, 2054000020,2054000000, 2052010080, 2052010060, 2052010040, 2052010020, 2052000020, 2052000000, 2050010080, 2050010060, 2050010040, 2050010020, 2050000020, 2050000000, 2048010080, 2048010060, 2048010040, Updated: 25 October 2013, Ocean-Wise, Using: EDINA Marine Digimap Service, https://digimap.edina.ac.uk, Downloaded: 2019-10-25 12:26:52.575, a.

Digimap. DiGSBS250K [SHAPE geospatial data], Scale 1:250000, Tiles: GB, Updated: 6 September 2011, BGS, Using: EDINA Geology Digimap Service, https://digimap.edina.ac.uk, Downloaded: 2019-12-05 15:24:22.171, b.

W. M. Drennan, P. K. Taylor, and M. J. Yelland. Parameterizing the sea surface roughness. *Journal of physical oceanography*, 35(5):835–848, 2005.

G. D. Egbert and S. Y. Erofeeva. Efficient inverse modeling of barotropic ocean tides. *Journal of Atmospheric and Oceanic Technology*, 19(2):183–204, 2002. ISSN 07390572. doi: 10.1175/1520-0426(2002)019⟨0183:EIMOBO⟩2.0.CO;2.

P. E. Farrell, D. A. Ham, S. W. Funke, and M. E. Rognes. Automated derivation of the adjoint of high-level transient finite element programs. *SIAM Journal on Scientific Computing*, 35(4):C369–C393, 2013.

J. Flowerdew, K. Horsburgh, C. Wilson, and K. Mylne. Development and evaluation of an ensemble forecasting system for coastal storm surges. *Quarterly Journal of the Royal Meteorological Society*, 136:1444–1456, 2010. ISSN 00359009. doi: 10.1002/qj.648.

J. Flowerdew, K. Mylne, C. Jones, and H. Titley. Extending the forecast range of the uk storm surge ensemble. *Quarterly Journal of the Royal Meteorological Society*, 139(670):184–197, 2013.

S. W. Funke. *The automation of PDE-constrained optimisation and its applications*. PhD thesis, Imperial College London, 2012.

C. Geuzaine and J. F. Remacle. Gmsh: A 3-D finite element mesh generator with built-in pre- and post-processing facilities. *International Journal for Numerical Methods in Engineering*, 79(11):1309–1331, 2009. ISSN 00295981. doi: 10.1002/nme.2579.

Z. Goss, D. Coles, and M. Piggott. Identifying economically viable tidal sites within the alderney race through optimization of levelized cost of energy. *Philosophical Transactions of the Royal Society A*, 378 (2178):20190500, 2020.

I. D. Haigh, M. P. Wadey, T. Wahl, O. Ozsoy, R. J. Nicholls, J. M. Brown, K. Horsburgh, and B. Gouldby. Spatial and temporal analysis of extreme sea level and storm surge events around the coastline of the UK. *Scientific Data*, 3:1–14, 2016. doi: doi:10.1038/sdata.2016.107.

M. C. G. Hall, D. G. Cacuci, and M. E. Schlesinger. Sensitivity Analysis of a Radiative-Convective Model by the Adjoint Method, 1982. ISSN 0022-4928.

S. Hallegatte, C. Green, R. J. Nicholls, and J. Corfee-Morlot. Future flood losses in major coastal cities. *Nature Climate Change*, 3(9):802–806, 2013. ISSN 1758678X. doi: 10.1038/nclimate1979.

A. Heemink, E. Mouthaan, M. Roest, E. Vollebregt, K. Robaczewska, and M. Verlaan. Inverse 3D shallow water flow modelling of the continental shelf. *Continental Shelf Research*, 22(3):465–484, feb 2002. ISSN 0278-4343. doi: 10.1016/S0278-4343(01)00071-1. URL `https://www.sciencedirect.com/science/article/pii/S0278434301000711`.

T. Kärnä, S. C. Kramer, L. Mitchell, D. A. Ham, M. D. Piggott, and A. M. Baptista. Thetis coastal ocean model: Discontinuous Galerkin discretization for the three-dimensional hydrostatic equations. *Geoscientific Model Development*, 11(11):4359–4382, 2018. ISSN 19919603. doi: 10.5194/gmd-11-4359-2018.

S. Kramer, T. Kärnä, J. Hill, and S. W. Funke. stephankramer/uptide: First release of uptide v1.0, 2020. `http://doi.org/10.5281/zenodo.3909652`.

R. W. Lardner, A. H. Al-Rabeh, and N. Gunay. Optimal Estimation of Parameters for a Two-Dimensional Hydrodynamical Model of the Arabian Gulf. *Journal of Geophysical Research*, 98(C10):18229–18242, 1993.

Y. Li, S. Peng, J. Yan, and L. Xie. On improving storm surge forecasting using an adjoint optimal technique. *Ocean Modelling*, 72:185–197, dec 2013. ISSN 1463-5003. doi: 10.1016/J.OCEMOD.2013.08.009. URL `https://www.sciencedirect.com/science/article/pii/S1463500313001625`.

M. Losch and P. Heimbach. Adjoint sensitivity of an ocean general circulation model to bottom topography. *Journal of Physical Oceanography*, 37(2):377–393, 2007.

X. Lu and J. Zhang. Numerical study on spatially varying bottom friction coefficient of a 2D tidal model with adjoint method. *Continental Shelf Research*, 26(16):1905–1923, oct 2006. ISSN 0278-4343. doi: 10.1016/J.CSR.2006.06.007. URL `https://www.sciencedirect.com/science/article/pii/S027843430600210X`.

S. Massmann. Sensitivities of an adjoint, unstructured mesh, tidal model on the European Continental Shelf. *Ocean Dynamics*, 60(6):1463–1477, dec 2010. ISSN 16167341. doi: 10.1007/s10236-010-0347-6. URL `https://doi.org/10.1007/s10236-010-0347-6`.

S. K. Mitusch, S. W. Funke, and J. S. Dokken. dolfin-adjoint 2018.1: automated adjoints for FEniCS and Firedrake. *Journal of Open Source Software*, 4(38), 2019.

W. Nowak. Using algorithmic differentiation for uncertainty analysis. In *22nd Telemac & Mascaret User Club*, pages 52–57, 2015. doi: 10.5281/zenodo.165522.

C. Pain, M. Piggott, A. Goddard, F. Fang, G. Gorman, D. Marshall, M. Eaton, P. Power, and C. De Oliveira. Three-dimensional unstructured mesh ocean modelling. *Ocean Modelling*, 10(1-2):5–33, 2005.

F. Rathgeber, D. A. Ham, L. Mitchell, M. Lange, F. Luporini, A. T. McRae, G. T. Bercea, G. R. Markall, and P. H. Kelly. Firedrake: Automating the finite element method by composing abstractions. *ACM Transactions on Mathematical Software*, 43(3), 2016. ISSN 15577295. doi: 10.1145/2998441.

J. Staneva, V. Alari, Ø. Breivik, J.-R. Bidlot, and K. Mogensen. Effects of wave-induced forcing on a circulation model of the north sea. *Ocean Dynamics*, 67(1):81–101, 2017.

T. Stocker, D. Qin, G.-K. Plattner, M. Tignor, S. Allen, J. Boschung, A. Nauels, Y. Xia, V. Bex, and P. M. (eds.). *IPCC, 2013: Climate Change 2013: The Physical Science Basis. Contribution of Working Group I to the Fifth Assessment Report of the Intergovernmental Panel on Climate Change*. Cambridge University Press, Cambridge, United Kingdom and New York, NY, USA, 2013.

A. Verdy, M. R. Mazloff, B. D. Cornuelle, and S. Y. Kim. Wind-driven sea level variability on the california coast: An adjoint sensitivity analysis. *Journal of physical oceanography*, 44(1):297–318, 2014.

C. Villaret, R. Kopmann, D. Wyncoll, J. Riehme, U. Merkel, and U. Naumann. First-order uncertainty analysis using Algorithmic Differentiation of morphodynamic models. *Computers & Geosciences*, 90:144–151, may 2016. ISSN 0098-3004. doi: 10.1016/J.CAGEO.2015.10.012. URL `https://www.sciencedirect.com/science/article/pii/S0098300415300777`.

C. V. Vouriot, A. Angeloudis, S. C. Kramer, and M. D. Piggott. Fate of large-scale vortices in idealized tidal lagoons. *Environmental Fluid Mechanics*, 19(2):329–348, apr 2019. ISSN 15731510. doi: 10.1007/s10652-018-9626-4. URL `https://doi.org/10.1007/s10652-018-9626-4`.

M. P. Wadey, I. D. Haigh, R. J. Nicholls, J. M. Brown, K. Horsburgh, B. Carroll, S. L. Gallop, T. Mason, and E. Bradshaw. A comparison of the 31 January–1 February 1953 and 5–6 December 2013 coastal flood events around the UK. *Frontiers in Marine Science*, 2:84, 2015. ISSN 2296-7745. doi: 10.3389/fmars.2015.00084. URL `https://www.frontiersin.org/article/10.3389/fmars.2015.00084`.

S. C. Warder, K. J. Horsburgh, and M. D. Piggott. Understanding the contribution of uncertain wind stress to storm surge predictions. In *4th IMA International Conference on Flood Risk*, Swansea, 2019.

J. Williams and R. Flather. Interfacing the operational storm surge model to a new mesoscale atmospheric mode. 2000.

J. Williams, K. J. Horsburgh, J. A. Williams, and R. N. Proctor. Tide and skew surge independence: New insights for flood risk. *Geophysical Research Letters*, 43(12):6410–6417, 2016. ISSN 19448007. doi: 10.1002/2016GL069522.

C. Wilson, K. J. Horsburgh, J. Williams, J. Flowerdew, and L. Zanna. Tide-surge adjoint modeling: A new technique to understand forecast uncertainty. *Journal of Geophysical Research: Oceans*, 118(10): 5092–5108, 2013. ISSN 21699291. doi: 10.1002/jgrc.20364.

J. Zhang, X. Lu, P. Wang, and Y. P. Wang. Study on linear and nonlinear bottom friction parameterizations for regional tidal models using data assimilation. *Continental Shelf Research*, 31(6):555–573, apr 2011. ISSN 0278-4343. doi: 10.1016/J.CSR.2010.12.011. URL `https://www.sciencedirect.com/science/article/pii/S0278434310003857`.